Suppression of the unsteady vortex wakes of a circular cylinder pair by a doublet-like counter-rotation

Andre S. Chan[1,2] and Antony Jameson[2,*,†]

[1]*Hitachi Global Storage Technologies, 5600 Cottle Road, San Jose, CA 95193, U.S.A.*
[2]*Department of Aeronautics and Astronautics, Stanford University, Stanford, CA 94305, U.S.A.*

SUMMARY

The present investigation examines the suppression of unsteady, two-dimensional wake instabilities of a pair of identical circular cylinders, placed side-by-side normal to freestream at a low Reynolds number of 150. It is found that when the cylinders are counter-rotated, unsteady vortex wakes can be completely suppressed. At fast enough rotational speeds, a virtual elliptic body is produced by a closed streamline, strongly resembling a doublet potential flow. Copyright © 2009 John Wiley & Sons, Ltd.

1. INTRODUCTION

1.1. Background

The flow past a pair of identical circular cylinders has been used as a model by various investigators who were interested in the interaction of vortex wakes of multiple bluff bodies in freestream. The previous studies were mostly experimental. The present paper takes a numerical approach. After comparing our results with known experimental data for stationary cylinders, we investigate the use of counter-rotation to suppress wake instabilities.

It is well known that when a circular cylinder is placed in a uniform freestream an unsteady separation develops, leading to a von Kármán vortex street. In the low Reynolds number range of less than 194, the vortex wakes are purely two dimensional [1]. At higher Reynolds numbers, the wakes become more complex and three dimensional. When a pair of identical circular cylinders is

---

*Correspondence to: Antony Jameson, Department of Aeronautics and Astronautics, Stanford University, Stanford, CA 94305-4035, U.S.A.
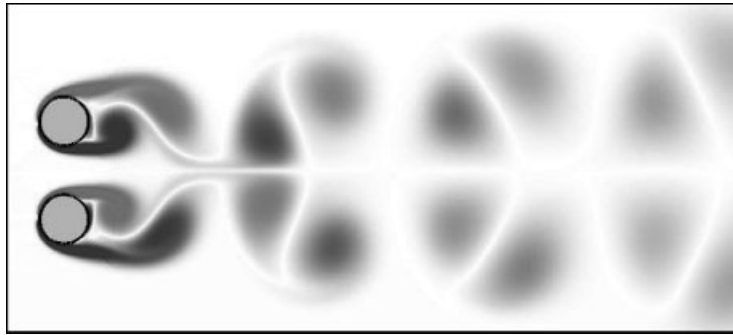†E-mail: jameson@baboon.stanford.edu

Figure 1. Contour plot of vorticity of an *anti-phase* vortex street past a circular cylinder pair, $Re_d = 150$, $g = 1$.

Figure 2. Contour plot of vorticity of an *in-phase* vortex street past a circular cylinder pair, $Re_d = 150$, $g = 1$.

placed side-by-side in a close proximity, there are strong interactions between the wakes. Following the work of Bearman and Wadcock [2] and Zdravkovich [3], Williamson [4] classified the vortex street of the cylinder pair into two categories—*anti-phase* and *in-phase*—for gap-to-diameter ratios in the range of $1.0 < g < 5.0$. As noted by Williamson, the anti-phase mode is predominant and stable. In this case each vortex lobe generally keeps its form while being gradually dissipated downstream of the bodies.

The results in this report have been obtained numerically with a commercial code, CFD-ACE+ from the ESI Corporation. Most commercial CFD codes today solve the incompressible Navier–Stokes equations using the original semi-implicit method for pressure-linked equations (SIMPLE) scheme developed by Patankar and Spalding [5] or one of its variants such as SIMPLE-C (consistent) and SIMPLE-R (revised). CFD-ACE+, uses the SIMPLE-C algorithm as proposed by Van Doormal and Raithby [6]. Details of the numerical implementation of SIMPLE-C in CFD-ACE+ can be found in the *User Manual* [7]. The first step of this study is to establish confidence in the numerical simulations by comparing the results of CFD-ACE+ with some well-known numerical and experimental work of previous investigators. Vortex interactions between a pair of cylinders are examined in the following paragraphs.

The CFD model used in this study uses between 150 000 and 200 000 computational cells depending on the physical geometry such as g, which dictates the way meshes are formed around the cylinders. The meshing pattern radiates from each cylinder in a geometrically progressive manner. The grid spacing next to the cylinder wall surface is approximately $0.004 \cdot d$. There are 280 grids circumferentially surrounding each cylinder surface.

Figure 1 illustrates the numerical result for the anti-phase mode, which Williamson experimentally observed as being stable. Figure 2 illustrates the in-phase vortex shedding mode, which Williamson found to be unstable. Each 'binary' pair of like-sign vortices tends to coalesce into a larger single vortex cell before eventually being dissipated far downstream. To obtain a numerical result for the in-phase mode, we found that one can use the technique of perturbing the flow velocity by artificially injecting a non-streamwise component into the computational domain for a few time steps. The purpose is to 'trip' the flow so that the non-streamwise component will encourage the flow to develop into an in-phase pattern. Another method that proved successful is to artificially increase the time step Δt and/or limit the convergence criteria so that the residual error builds up for a few time steps. When Δt is throttled back down and a reasonable convergence criterion is re-established (typically a reduction of the residual errors by four orders of magnitude), the resulting initial disturbance tends to encourage the in-phase instability to form. The results of these simulations verify the capability of CFD-ACE+ to predict wake instabilities at a Reynolds number of 150. Moreover simulations at the Reynolds number of 200 with $g=2.4$, as shown in Figures 3 and 4, predict wake patterns, which closely resemble the patterns observed by Williamson in his experiment, as can be seen in Figures 6(a) and (b) of his report [4]. For these simulations, we set up the boundary conditions to replicate the channel width, length and blockage factor used in Williamson's experiment. Further validation of the numerical method is also provided in the Appendix, which presents comparisons of our numerical simulations with available numerical and experimental data for flows past a single cylinder.

1.2. Configurations of a counter-rotating circular cylinder pair

The main body of the paper focuses on flows over counter-rotating cylinders. According to Williamson, flow instabilities occur in the wakes of a pair of stationary cylinders with $g=1$ in the Reynolds number range above 55. He also reports that the wakes remain two dimensional at a Reynolds number of 200. If cylinders are rotated at the same speed but in opposite directions, there is the possibility of stabilizing the wakes. It is also conceivable that a flow pattern similar to a doublet in the potential flow theory can be produced. We focus our analysis on the control of two-dimensional vortex wakes in a Reynolds number range below the onset of three-dimensional effects. Specifically, we choose $Re_d=150$ and $g=1$ as a basis of flow for our current numerical experiments. There are two possible configurations:

(1) A doublet-like direction (Figure 5)—top cylinder rotates clockwise and bottom counterclockwise at the same speed, ω.
(2) A reverse-doublet-like direction (Figure 6)—top cylinder rotates counter-clockwise and bottom clockwise at the same speed, ω.

We also define the magnitude of the cylinder rotation as $\Omega=2 \cdot U/d$. Thus, if we rotate each cylinder at a speed of $\omega=1\Omega$, it means that the surface velocity magnitude of the cylinder is exactly equal to the uniform velocity magnitude.
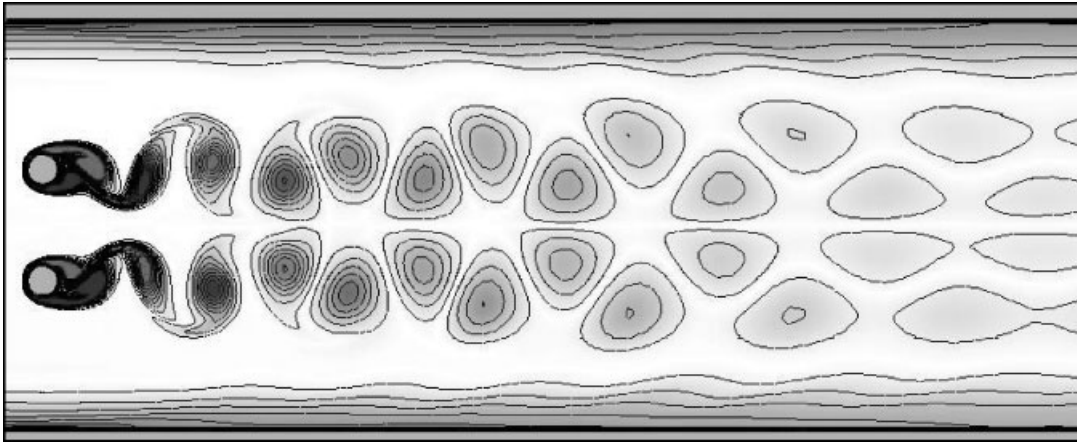
Figure 3. Iso-contour plot of vorticity of an *anti-phase* vortex street past a circular cylinder pair, $Re_d = 200$, $g = 2.4$, for direct comparison with Williamson [4].

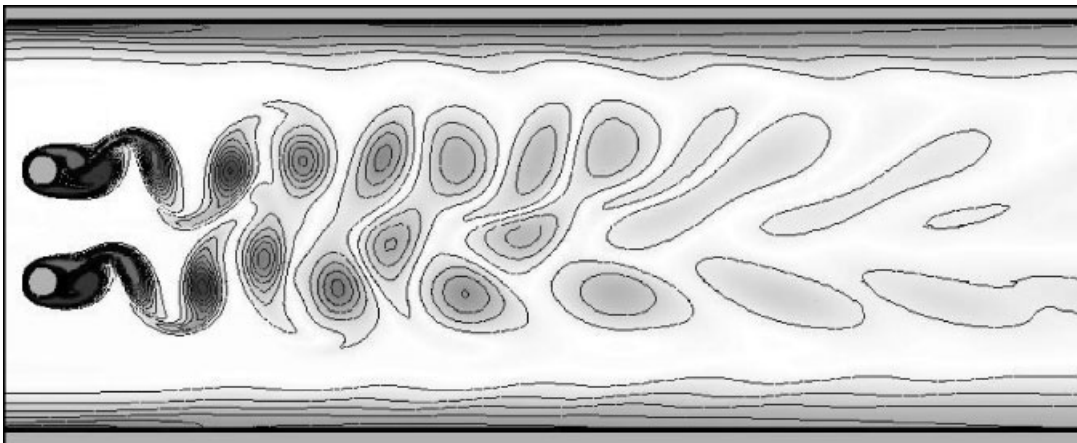Figure 4. Iso-contour plot of vorticity of an *in-phase* vortex street past a circular cylinder pair, $Re_d = 200$, $g = 2.4$, for direct comparison with Williamson [4].

2. NUMERICAL RESULTS FOR COUNTER-ROTATING CYLINDERS

2.1. A doublet-like rotating circular cylinder pair

Figures 7(a) and (b) show a comparison of the instantaneous vorticity of a pair of counter-rotating cylinders in a doublet-like mode with that of a non-rotating pair of cylinders in the in-phase shedding mode. We used the results from the in-phase shedding case of the non-rotating cylinder to start the flow of the rotating case. In the case of $g = 1$ at $Re_d = 150$, it is apparent that the rotation causes the wakes to coalesce much sooner than the non-rotating case. It is also clear that the unsteady vortex wakes shed off each rotating cylinder are significantly attenuated. The reduction in
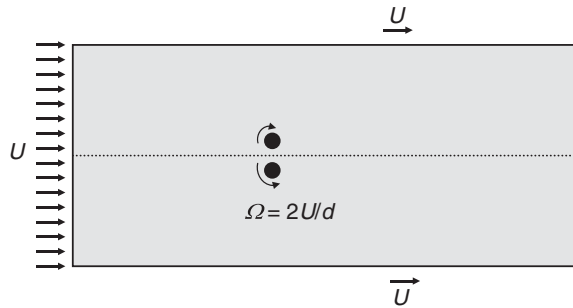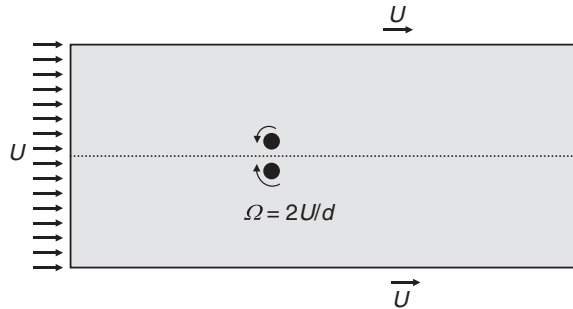
Figure 5. A doublet-like configuration.

Figure 6. A reverse-doublet-like configuration.

the fluctuating lift and drag, plotted against non-dimensional time, $\tau = t \cdot d / U$, is shown on Figures 8(a) and (b). It can be seen from the spread of the lift coefficients between the upper and lower cylinders that the rotation has the effect of pushing the cylinders apart. The rotation also helps streamline the flow, producing a reduction in the drag coefficient of each cylinder, leading to a reduction in the total force on both cylinders. Both the predicted behavior of the vortex wakes and the reduction in flow-induced forces on the bodies seem to be in a reasonable agreement with the recently reported results of Yoon *et al.* [8].

2.2. Symmetrical steady shedding

When the rotational speed is further increased the vortex wakes can be completely suppressed as seen on Figure 9, which plots the streamlines to illustrate the evolution of steady wakes as a function of rotational speed. It appears that the flow past a circular cylinder pair stops shedding unsteady vortex wakes at a rotational speed between 1Ω and 1.5Ω. When a steady flow is produced by rotation, the entire force fluctuation on each cylinder is totally suppressed and, as a result, the total sum of the lift coefficient, C_L, of the cylinder pair is exactly zero. Somewhere between the rotational speeds of 2.5Ω and 2.75Ω, a closed vortex system is formed similar to a potential doublet in a form of virtual elliptic body (Figure 12). Figures 10(a) and (b) showthe lift and
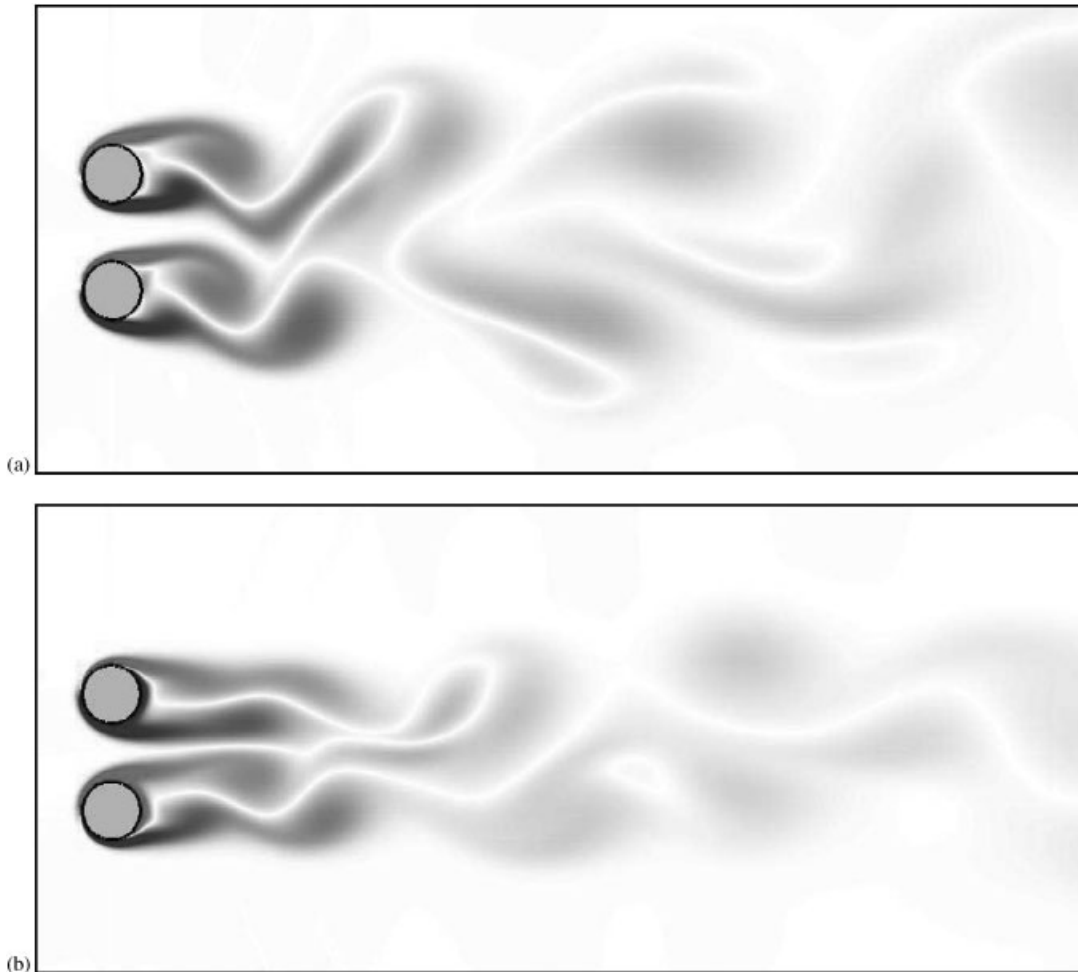
Figure 7. (a) Vorticity plot of flow in an in-phase mode past a non-rotating pair of circular cylinders, $Re_d = 150$, $g = 1$ and (b) vorticity plot of flow in an in-phase mode past a doublet-like pair of circular cylinders counter-rotating at $\omega = 1\Omega$, $Re_d = 150$, $g = 1$.

drag coefficients of a doublet-like rotating circular cylinder pair when steady flow is reached. The total lift coefficient C_L is zero, while the total drag coefficient C_D of the circular cylinder pair is significantly reduced as the rotational speed is increased. Because the flow is symmetric along the horizontal center line (half way between the two cylinders), the drag coefficient of the top cylinder must be precisely the same as that of the bottom cylinder. The form drag becomes negative when the rotational velocity is increased beyond 1.8Ω (Figure 11). Remarkably, the total drag coefficient is slightly negative at a rotational speed of 2.5Ω, indicating that the work that is put into rotating the cylinder not only stabilizes the flow, but can be converted into forward thrust. Thus the rotational speed is increased beyond 2.5Ω and a virtual elliptic body appears, the form drag starts to increase as the size of the virtual body increases. The total drag remains small,
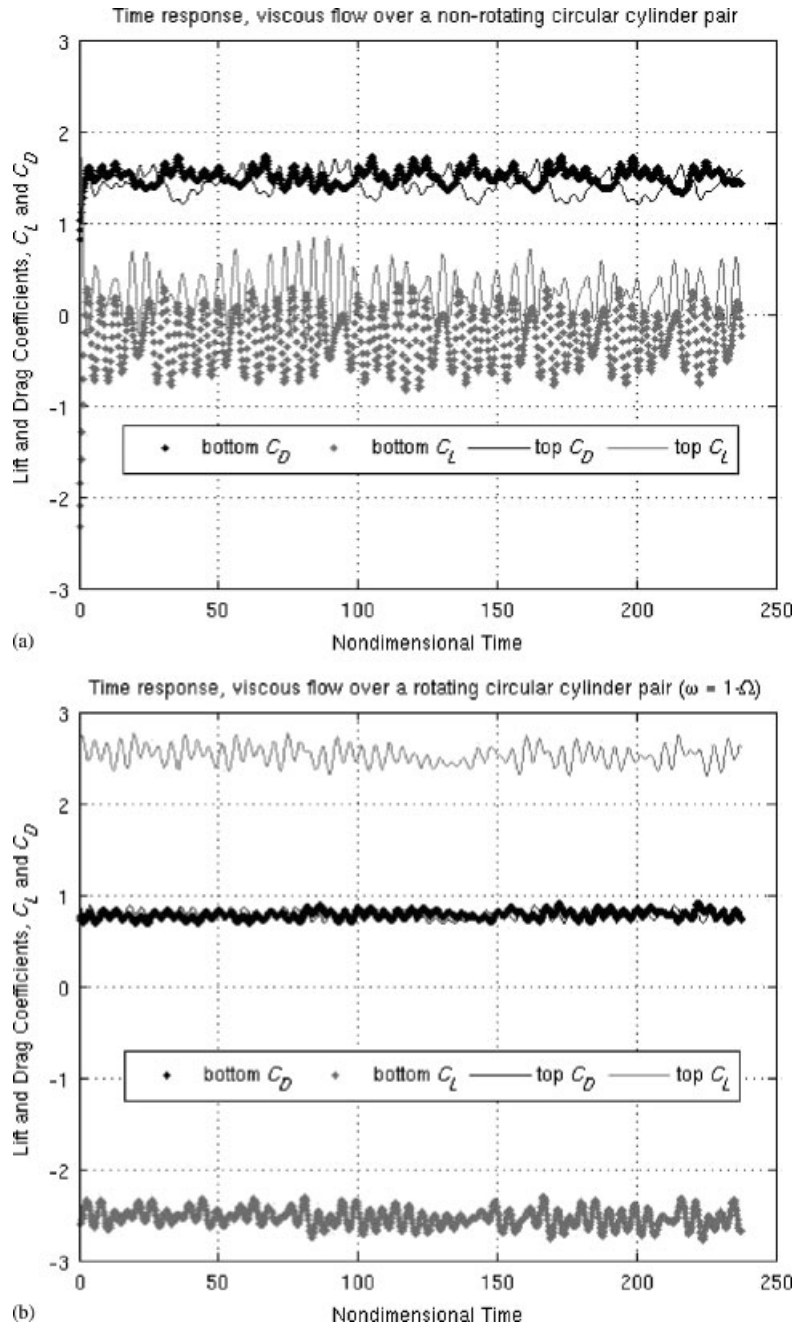
Figure 8. Time response of lift and drag coefficients of each circular cylinder: (a) non-rotating pair, $Re_d = 150$, $g = 1$ and (b) doublet-like counter-rotating pair, $\omega = 1\Omega$, $Re_d = 150$, $g = 1$.
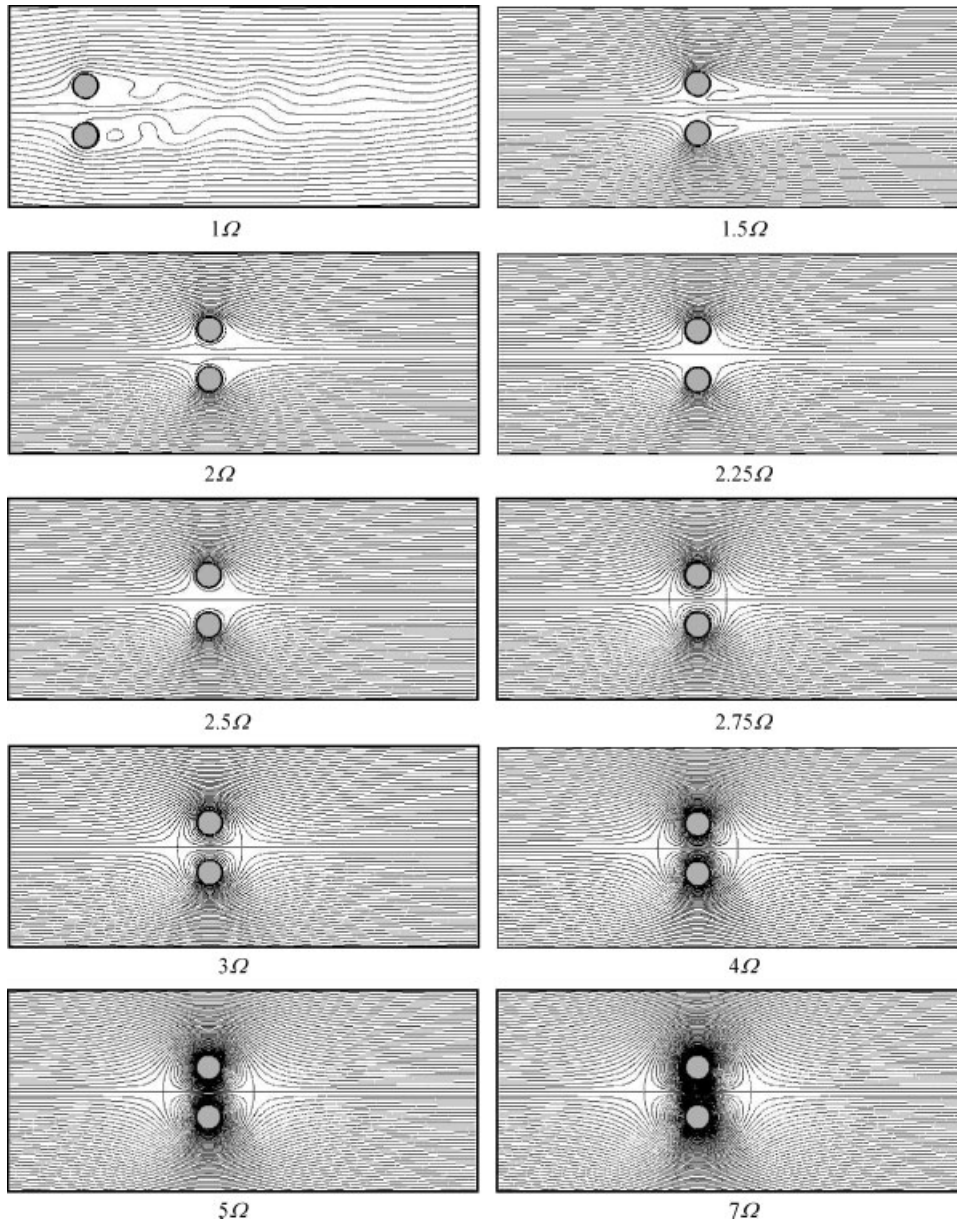
Figure 9. Streamlines showing the evolution of steady flow with increasing rotational speeds, $Re_d = 150$, $g = 1$. (Unsteady flow: 1Ω; Steady flow: 1.5Ω, 2Ω, 2.25Ω, 2.5Ω, 2.75Ω, 3Ω, 4Ω, 5Ω and 7Ω).

however, because the frictional contribution to the horizontal force starts to decrease at about the same rate. Both contributions change sign at a rotational speed around 4.3Ω, and eventually as the rotational speed is further increased, net thrust is again observed.

Steady lift coefficient produced by a doublet-like pair counter-rotating circular cylinders

(a)

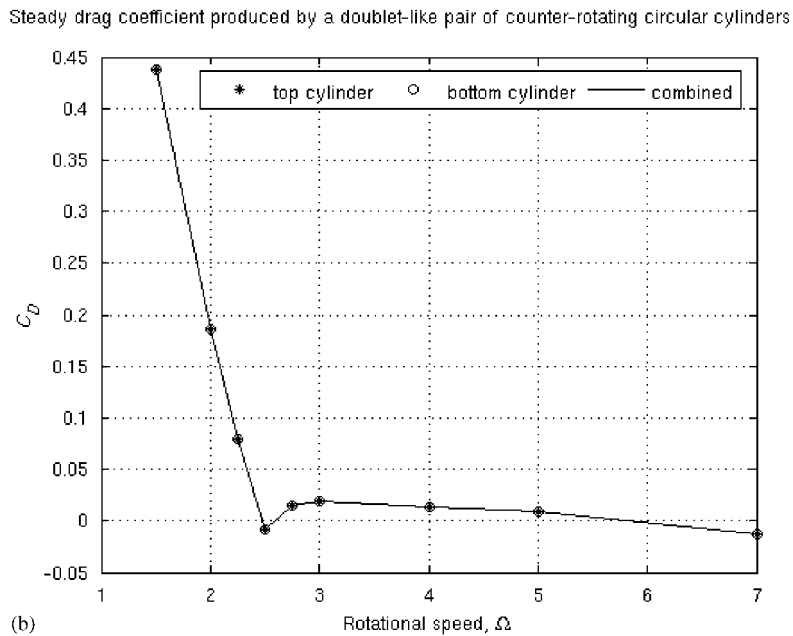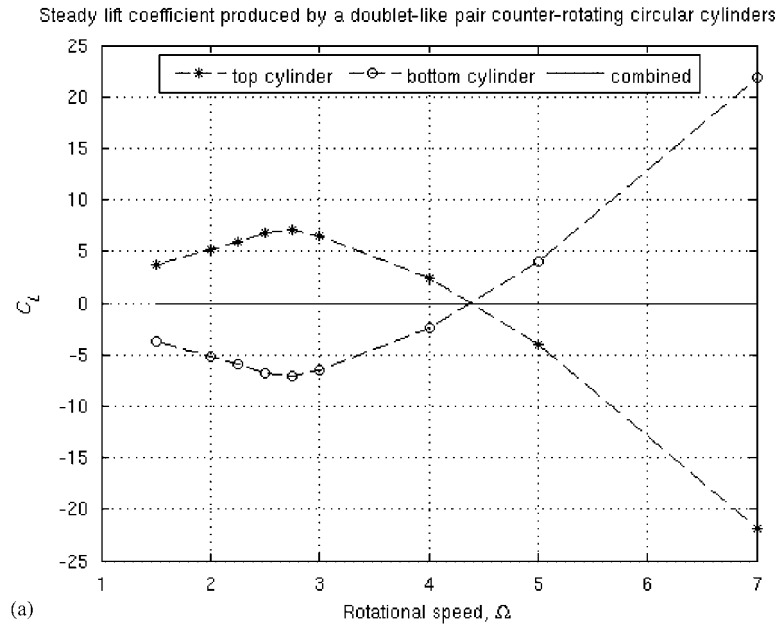Steady drag coefficient produced by a doublet-like pair of counter-rotating circular cylinders

(b)

Figure 10. (a) Lift coefficient of a pair of counter-rotating circular cylinders (steady flow), $Re_d = 150$, $g = 1$ and (b) drag coefficient of a pair of counter-rotating circular cylinders (steady flow), $Re_d = 150$, $g = 1$.

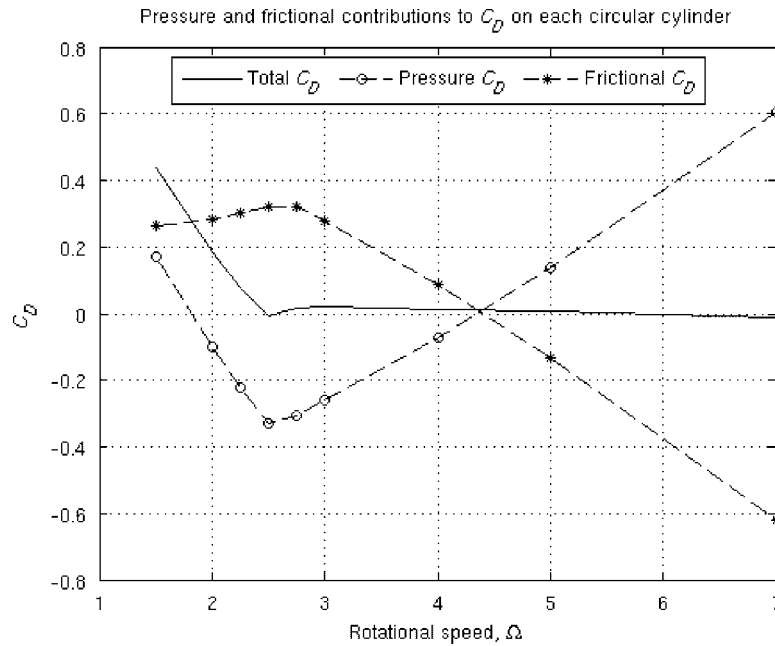Pressure and frictional contributions to C_D on each circular cylinder

Figure 11. Pressure and frictional contributions to C_D on each circular cylinder (steady flow), $Re_d = 150$, $g = 1$.

2.3. A reverse-doublet-like rotating circular cylinder pair

One may also ask whether a steady flow solution can be produced if the cylinders rotate in a reverse-doublet direction (Figure 6). In the reverse direction, vortex wakes from the top and bottom cylinders are forced apart so that the chance of the vortex streets interfering with each other rapidly diminishes with increasing rotational speeds. This lessens the ability to attenuate vortex wakes as compared with the more effective doublet-like rotation. From our study, we confirmed that a steady flow can be achieved at an approximate rotational speed of 3.5Ω and upwards. We also noticed that C_D is generally higher than when the cylinders are rotated in the doublet direction. The two cylinders are also attracted by opposing vertical forces of equal magnitude, which increase with the speed (Figure 13).

3. CONCLUSION

In this report we have demonstrated by numerical simulation that unsteady vortex wakes can be completely suppressed by counter-rotating a pair of cylinders. There are essentially two possible directions of counter rotation—a doublet-like direction and the reverse. We have found that when the cylinder pair is rotated in a doublet-like direction, a significant drag reduction can be achieved, and at high enough speeds a virtual elliptic body is formed. In the speed range from where the steady flow first develops (1.5Ω) to where the virtual elliptic body is first observed (2.75Ω), drag reduction is achieved mostly due to the decrease in form drag, which
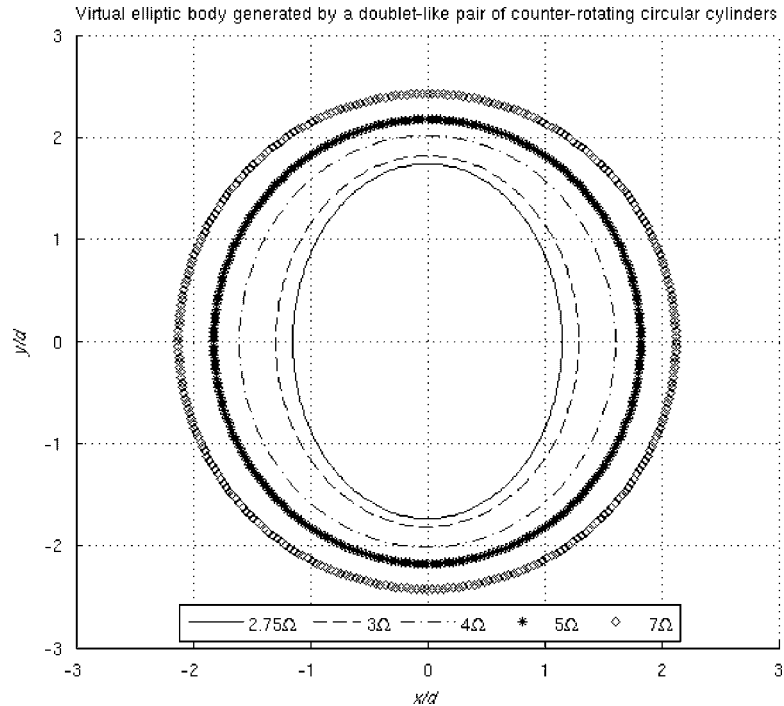
Figure 12. Virtual elliptic body (closed vortex system) at various rotational speeds, $Re_d = 150$, $g = 1$.

actually becomes negative in the range beyond 1.8Ω. At higher rotational speeds, the form drag starts to increase again and becomes positive beyond 4.3Ω. However, the total drag remains low because the frictional contribution to the horizontal force exhibits the opposite trend. The net positive thrust is observed at rotational speed of 2.5Ω, and again at very high rotational speeds. Unsteady vortex wakes can also be completely suppressed by rotating the cylinder pair in the reverse-doublet-like direction. This is not as effective, however, as the doublet direction. It takes approximately 3.5Ω to achieve steadiness, while the drag coefficient of each cylinder remains high.

We have also verified our results with two other codes—another commercial solver (STAR-CD), and a higher-order spectral difference scheme developed by Liang *et al.* for simulation of compressible viscous flow [9]. In the latter case simulations were performed at a Mach number of 0.1. Both of these codes verify the formation of a virtual elliptic body at high rotational speeds. They also confirm a reduction in drag with increasing rotational speed, and finally the production of thrust as predicted in this work. However, it is not easy to quantify the accuracy of the force predictions. With the settings we used, CFD-ACE+ is nominally close to second-order accuracy. We have generally worked with a mesh density that was sufficient to give accurate results in a previous study of flows past a single stationary cylinder, for which experimental data were available. We are also collaborating with researchers in Princeton University to verify our predictions by an experimental investigation of flows past counter-rotating cylinders. We plan further investigation with various geometric gaps between the cylinders. We also plan to investigate

3.5Ω: $C_D = 0.52$ (top and bottom), $C_L = 13.64$ (bottom), $C_L = -13.64$ (top)

3.75Ω: $C_D = 0.45$ (top and bottom), $C_L = 15.55$ (bottom), $C_L = -15.55$ (top)

5Ω: $C_D = 0.14$ (top and bottom), $C_L = 27.11$ (bottom), $C_L = -27.11$ (top)
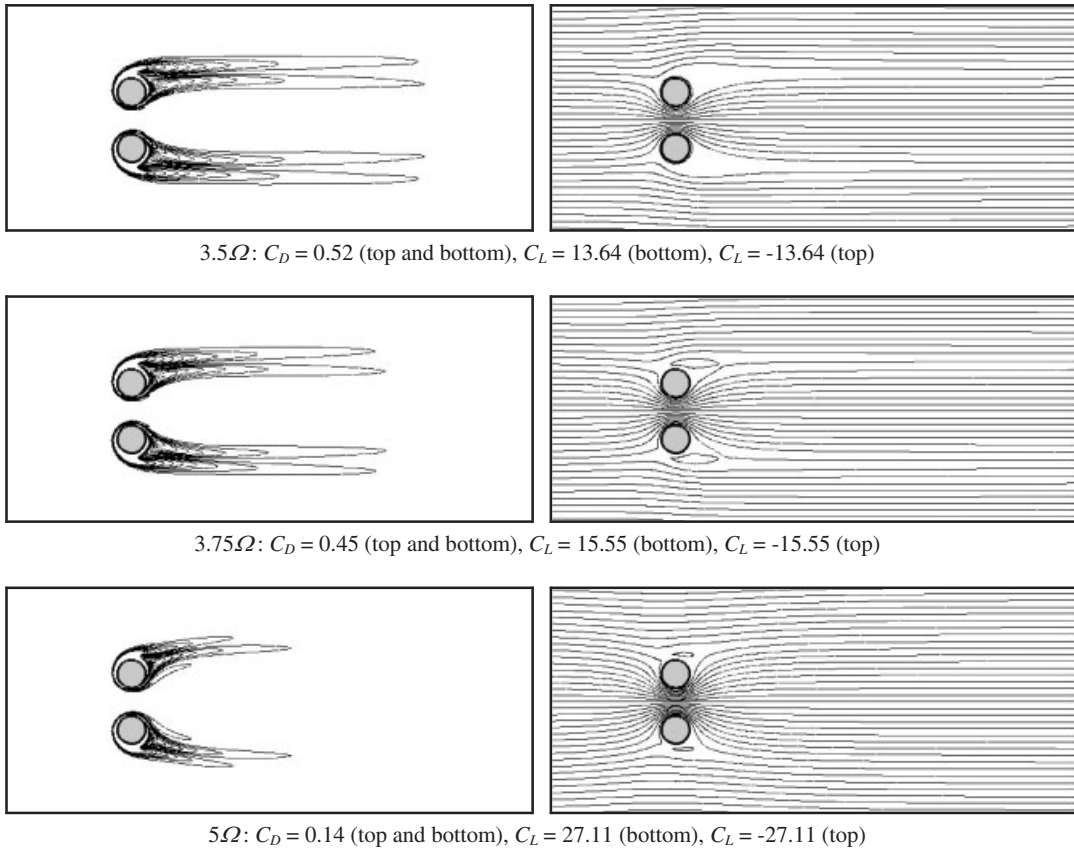
Figure 13. Flow patterns of a reverse-doublet-like circular cylinder pair counter-rotating at selected speeds: vorticity (left column), streamlines (right column), $Re_d = 150$, $g = 1$.

asymmetric configurations, including cases in which the cylinders are counter-rotated at different speeds, and cases in which the cylinders have different diameters.

APPENDIX A

In order to reinforce confidence in the results obtained with CFD-ACE+, we present some comparisons with other known experimental and numerical results from the work of Williamson [1] and Belov *et al.* [10, 11]. We focus on the unbounded flow past a circular cylinder at $Re_d = 150$, taking the numerical result of Belov as a baseline for comparison. Our modified O-mesh is shown on an x-y Cartesian coordinate system in Figure A1.

Our simulation uses the same number of computational cells as Belov, 256×256. While the circumferential spacing is uniform, the normal spacing is increased geometrically with the grid layer next to cylinder surface being $0.0003 \cdot d$, which is the same as that used by Belov. It should also be noted that Belov used a central differencing scheme (CDS) for the convection term,
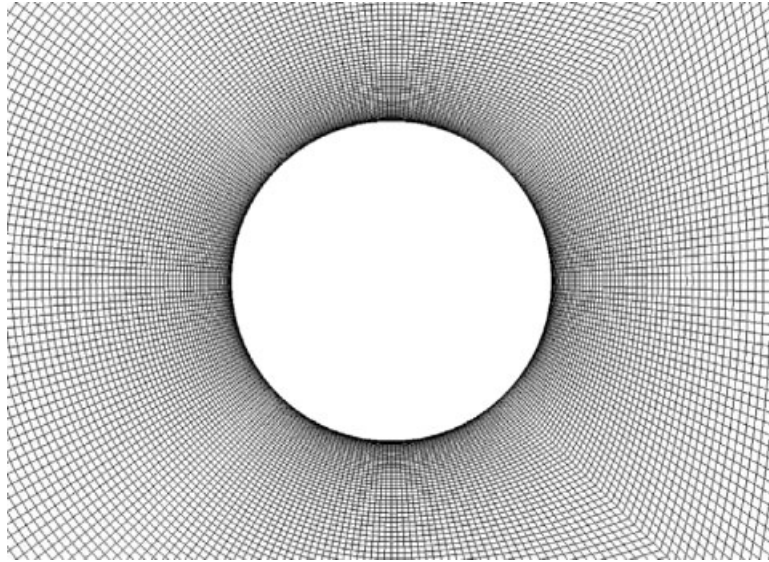
Figure A1. Modified O-mesh around circular cylinder.

together with a third-order artificial dissipation term similar to that used by Farmer [12]. For time discretization, Belov implemented the second-order accurate implicit backward difference scheme

$$\frac{\mathrm{d}\phi}{\mathrm{d}t} \approx \frac{3\phi^{n+1} - 4\phi^n + \phi^{n-1}}{2\Delta t}$$

CFD-ACE+ offers options for time discretization by the Crank–Nicolson (CN) scheme and a first-order backward Euler scheme. When using the CN scheme, we found that spatial discretization with the 2nd order upwind difference scheme (2UDS) and CDS produce very similar results. Qualitatively, the instantaneous plot of the z-component of vorticity, shown on Figure A2, reveals the typical von Kármán vortex street as one would expect from flow past a circular cylinder at $Re_d = 150$. It shows the formation of two rows of alternating vortices in the wake of the cylinder. This asymmetrical flow pattern produces an oscillating pressure distribution (Figure A3) on the cylinder, and leads to fluctuating C_L and C_D. Note that C_D oscillates twice as fast as C_L. The shedding pattern is regular but is subjected to viscous dissipation as each vortex moves further downstream away from the obstructing body. The rate of decay may be exaggerated in the simulations due to numerical dissipation. However, no spurious reflection is observed downstream confirming the correct pressure setting at the far right boundary.

When a first-order backward Euler scheme is used for time discretization, the Strouhal number as well as the amplitudes of the drag and lift coefficients are significantly different. Figures A4 and A5 illustrate the difference between the solutions obtained from the backward Euler scheme as compared with that from CN. Note that the plots correspond to flow solutions in which the steady asymmetric shedding characteristics are established. One of the techniques used to accelerate the shedding is to perturb the initial condition by using very large Δt (e.g. 0.1) in the first few steps. Once the mean flow is established throughout the domain, Δt is then throttled back to the desired target (e.g. 0.0001 s).
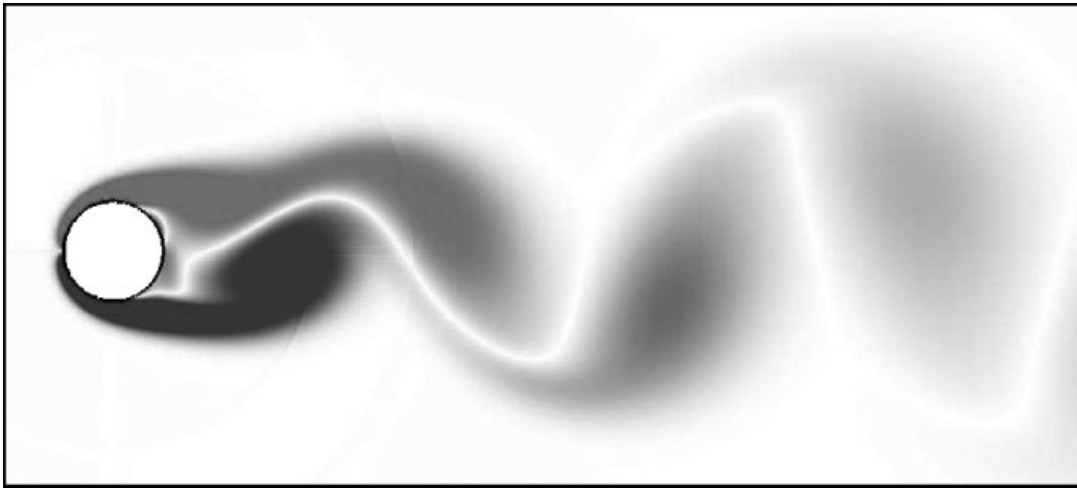
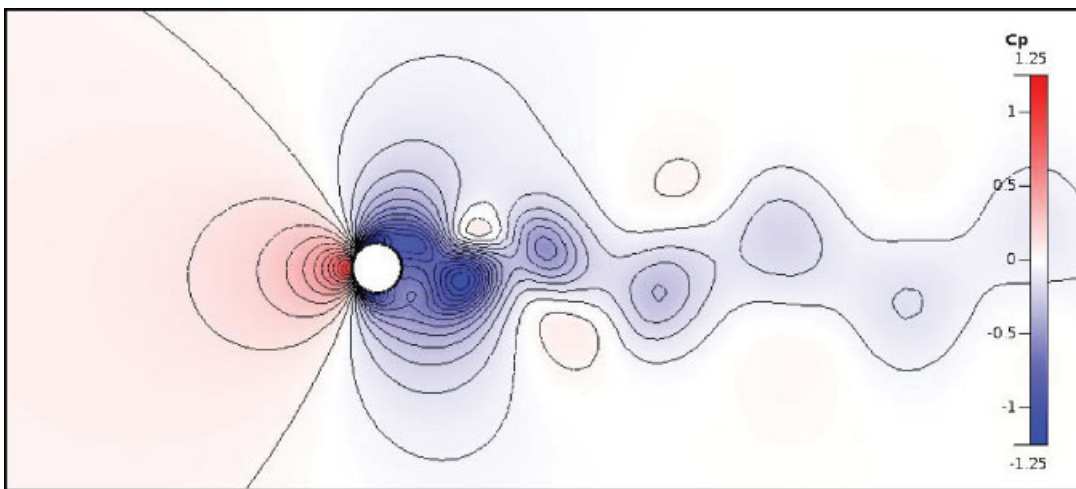Figure A2. Instantaneous plot of vorticity of flow past a circular cylinder, 2UDS, CN, $Re_\mathrm{d} = 150$.

Figure A3. Instantaneous Cp plot showing isobar of flow past a circular cylinder, 2UDS, CN, $Re_\mathrm{d} = 150$.

The shortcomings of the first-order time discretization become even more apparent in solutions on coarser grids. We have investigated coarser grids in the interest of saving computational time to enable the study of numerous variations. Table AI shows the comparison of the results for flow past a singular circular cylinder at $Re_\mathrm{d} = 150$ using these different schemes. It is obvious that the accuracy of St and C_{pb} suffers markedly when the backward Euler scheme is used. Thus, the 2UDS and the CN scheme have been chosen for our study of wake flow behind a pair of cylinders. It is noted that a coarse mesh can produce reasonable results when the proper temporal and spatial differencing schemes are used.
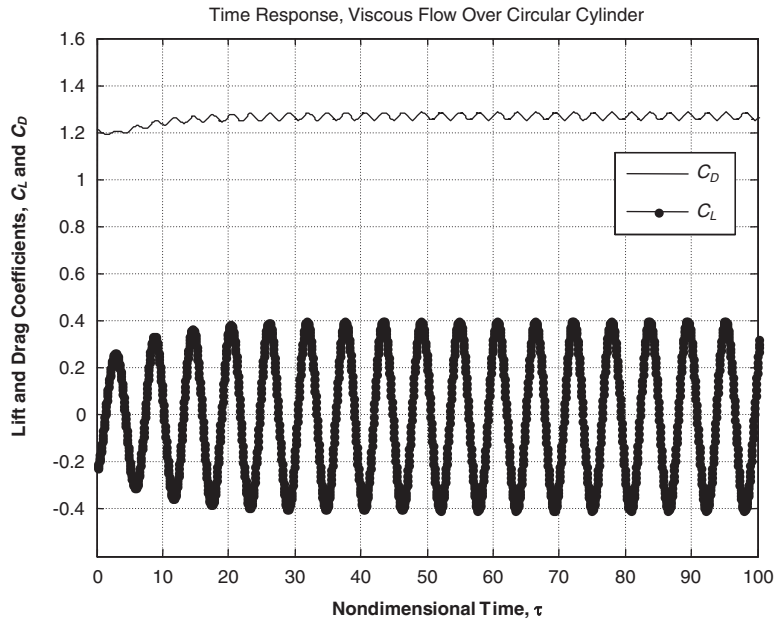
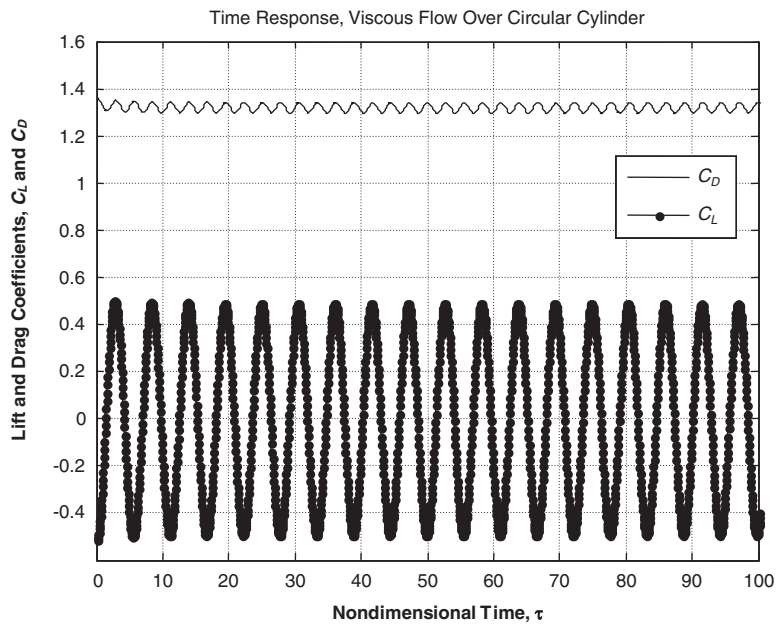Figure A4. C_L and C_D of flow past a circular cylinder, unbounded, 2UDS, Euler.

Figure A5. C_L and C_D of flow past a circular cylinder, unbounded, 2UDS, CN.

Table AI. Comparison of properties for flow past a circular cylinder at $Re_d = 150$.

| Source	Total cells	C_L	C_D	St	C_{pb}
Belov [10, 11]	65 536	0.000 ± 0.486	1.168 ± 0.025	0.182	-0.85
2UDS, Euler	65 536	0.000 ± 0.401	1.268 ± 0.017	0.174	-0.73
CDS, CN	65 536	0.000 ± 0.531	1.331 ± 0.028	0.181	-0.80
2UDS, CN	65 536	0.000 ± 0.492	1.319 ± 0.023	0.180	-0.79
2UDS, Euler (Coarse)	27 200	0.000 ± 0.146	1.132 ± 0.002	0.154	-0.57
CDS, CN (Coarse)	27 200	0.000 ± 0.439	1.281 ± 0.019	0.175	-0.76
2UDS, CN (Coarse)	27 200	0.000 ± 0.411	1.278 ± 0.017	0.174	-0.75
Williamson, exp. [1]	—	—	—	0.184	-0.86
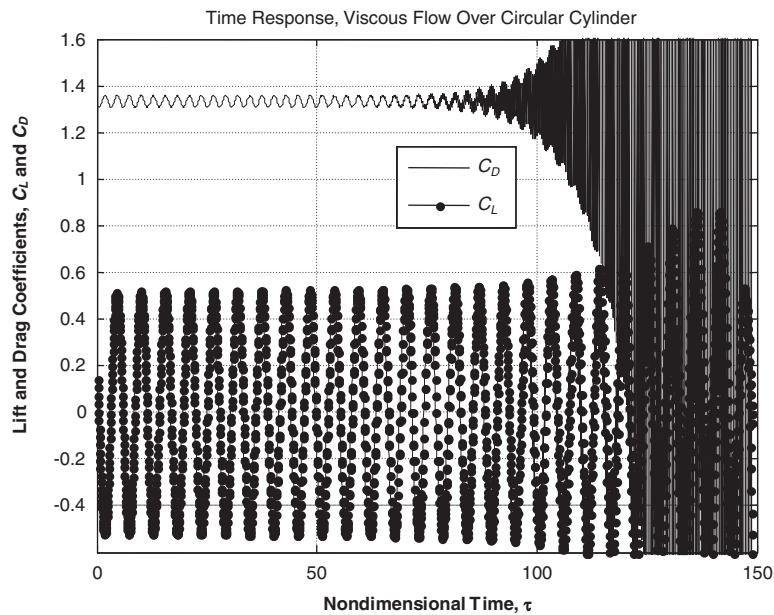
Figure A6. Numerical oscillation appears in flow solution using traditional
Crank–Nicolson scheme (i.e. blending factor = 0.5).

It is well known that the CN scheme can sometimes lead to non-physical, oscillatory solutions when the time step Δt is set too large. In the interest of saving computational time, we aim to use the largest possible time step that will not produce oscillations. CFD-ACE+ allows a biasing scheme where the two-level time discretization can be modified so that the code will solve the solution with more or less implicit information. For example, when the blending factor (also known as weighting or biasing factor) is set to 0.5, it produces the traditional CN scheme where the variables at time step n and $n+1$ have equal weighting of first-order explicit and backward implicit Euler schemes. When it is set to 1.0, it recovers the implicit Euler method. The blending scheme employed in the code essentially follows the theta method used for solving initial value problems
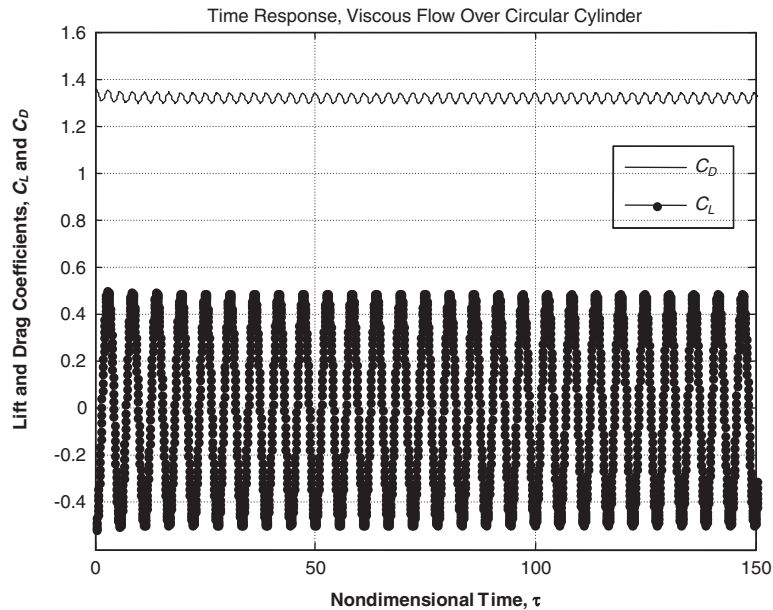
Figure A7. Flow solution with blending factor of 0.6.

of stiff systems of differential equations. It has been found by Prothero and Robinson [14] and Berzins and Furzeland [13] that a factor of 0.55 produces accurate and stable results for large non-linear systems of stiff equations. We have found that a default setting of 0.6 is sufficient to inhibit oscillation in the solutions. Figure A6 shows a diverged solution when the pure CN scheme (blending factor = 0.5) is used with $\Delta t = 0.0001$, while Figure A7 shows a stable solution with no significant deviation in C_D, C_L, or St from the references when the blending factor is set at 0.6.

NOMENCLATURE

C_D	drag coefficient
C_L	lift coefficient
C_{pb}	base pressure coefficient at 180° from the front stagnation point
d	diameter of circular cylinder
g	gap (between two circular cylinders) to diameter ratio
Re_d	Reynolds number based on diameter of a circular cylinder
St	Strouhal number
t	real time
U	uniform freestream velocity
Δt	time step
ω	rotational velocity magnitude of circular cylinder
Ω	rotational velocity magnitude of circular cylinder at $2 \cdot U/d$
τ	non-dimensional time, $t \cdot U/d$

REFERENCES

1. Williamson CHK. Vortex dynamics in the cylinder wake. *Annual Review of Fluid Mechanics* 1996; **28**:477–539.
2. Bearman PW, Wadcock AJ. The interaction between a pair of circular cylinders normal to a stream. *Journal of Fluid Mechanics* 1973; **61**:499–511.
3. Zdravkovich M. Review of flow interference between two circular cylinders in various arrangements. *Transactions of ASMEI: Journal of Fluids Engineering* 1977; **99**:618–633.
4. Williamson CHK. Evolution of a single wake behind a pair of bluff bodies. *Journal of Fluid Mechanics* 1985; **159**:1–18.
5. Patankar SV, Spalding DB. A calculation procedure for heat, mass and momentum transfer in three-dimensional parabolic flows. *International Journal of Heat and Mass Transfer* 1972; **15**:1787–1806.
6. Van Doormal JP, Raithby GD. Enhancements of the SIMPLE method for predicting incompressible fluid flows. *Numerical Heat Transfer* 1984; **7**:147–163.
7. ESI CFD Inc. CFD-ACE+ *V2008.2 User Manual*. ESI CFD Inc.: Huntsville, 2008.
8. Yoon HS, Kim JH, Chun HH, Choi HJ. Laminar flow past two rotating circular cylinders in a side-by-side arrangement. *Physics of Fluids* 2007; **19**(128103):1–4.
9. Liang C, Premasuthan S, Jameson A. High-order accurate simulation of low-Mach laminar flow past two side-by-side cylinders with spectral difference method. *ACL Report 2008-04*, Stanford University, 2008 (submitted to the *Fifth MIT Conference on Computational Fluid and Solid Mechanics*, June, 2009).
10. Belov A, Martinelli L, Jameson A. A new implicit algorithm with multigrid for unsteady incompressible flow calculations. *AIAA Paper* 1995; **95**:0049.
11. Belov A, Jameson A, Martinelli L. Three-dimensional unsteady incompressible flow calculations using multigrid. *AIAA Paper* 1997; **97**:0443.
12. Farmer R. A finite volume multigrid solution to the three dimensional nonlinear ship wave problem. *Ph.D. Thesis*, MAE Department, Princeton University, 1993.
13. Berzins M, Furzeland BM. An adaptive theta method for the solution of stiff and nonstiff differential equations. *Applied Numerical Mathematics* 1992; **9**:1–19.
14. Prothero A, Robinson A. On the stability and accuracy of one-step methods for solving stiff systems of ordinary differential equations. *Mathematics of Computation* 1974; **28**:145–162.